

NANO EXPRESS

Open Access



Coherent Light Photo-modification, Mass Transport Effect, and Surface Relief Formation in As_xS_{100-x} Nanolayers: Absorption Edge, XPS, and Raman Spectroscopy Combined with Profilometry Study

O. Kondrat^{1*}, R. Holomb¹, A. Csik², V. Takáts², M. Veres³ and V. Mitsa¹

Abstract

As_xS_{100-x} ($x = 40, 45, 50$) thin films top surface nanolayers affected by green (532 nm) diode laser illumination have been studied by high-resolution X-ray photoelectron spectroscopy, Raman spectroscopy, optical spectroscopy, and surface profilometry. It is shown that the composition of obtained films depends not only on the composition of the source material but as well on the composition of the vapor during the evaporation process. Near-bandgap laser light decreases both As–As and S–S homopolar bonds in films, obtained from thermal evaporation of the $As_{40}S_{60}$ and $As_{50}S_{50}$ glasses. Although $As_{45}S_{55}$ composition demonstrates increasing of As–As bonds despite to the partial disappearance of S–S bonds, for explanation of this phenomenon Raman investigations has also been performed. It is shown that As_4S_3 structural units (s.u.) responsible for the observed effect. Laser light induced surface topology of the $As_{45}S_{55}$ film has been recorded by 2D profilometer.

Keywords: As-S nanolayers, Photoinduced changes, XPS, Raman spectroscopy, Core level, Valence band, Mass transport, Chalcogenide thin films

Background

The research of chalcogenide glassy (ChG) materials formed a general understanding of electronic phenomena in disordered structures [1, 2]. The numerous investigations of their fundamental physical and chemical properties have been already performed [3–6]. Unique structural, electronic, and optical properties determined their various applications. The high infrared (IR) transparency of fibers on the basis of the ChG allows transmitting high-power IR light. The large refractive indices and third-order optical nonlinearities of the chalcogenide glasses make them the best candidates for the photonic devices for ultrafast all-optical switching and data processing [7].

Various applications have been proposed on the basis of the light sensitivity of non-crystalline chalcogenides, especially in amorphous thin film form [8–10]. Thus, photosensitivity is the main feature of chalcogenide glasses for phase-change memory, direct waveguides, and grating patterning.

The high-quality optical elements are required for the development of all-optical signal processing systems. Possibility of high-level integration of these elements in optical chips implies improved fabrication technology in order to achieve low optical losses at the near surface layers and the high level of laser damage threshold at femtosecond laser pulses. Also the large IR transparency or high optical nonlinearity of amorphous As–S binary systems make them a prospective optical media for the future ultrafast photonic systems. Our previous Raman studies of non-crystalline As–S binary system reveal the

* Correspondence: o.b.kondrat@gmail.com

¹Uzhhorod National University, Pidhirna Str. 46, Uzhhorod 88000, Ukraine
Full list of author information is available at the end of the article

differences between the structures of As_2S_3 films and bulk glass at nano-scale dimension [11]. The analysis shows that it is caused mainly by the phase separation, i.e., contribution of As_4S_4 cage-like molecules in the vapor during As_2S_3 thermal evaporation. In the further studies of the structure of amorphous As_2S_3 glasses and films using photon-energy-dependent Raman spectroscopy, the effect of laser-induced transformation of As_4S_4 molecules was observed [12]. Therefore, the As_4S_4 molecules can be classified as light absorption centers in As_2S_3 structure and leading to increasing the optical losses of an optical media.

The structure and properties of $\text{As}_{45}\text{S}_{55}$ glassy material and thin film were investigated earlier [13, 14]. Using macro FT-Raman spectroscopy, energy-dependent micro-Raman spectroscopy and first principle calculations established that the light-induced structural transformations in $\text{As}_{45}\text{S}_{55}$ glass take place mainly from alterations of As_4S_4 molecules in glass network. An impact of near-bandgap laser illumination transforms $\alpha(\beta)\text{-As}_4\text{S}_4$ molecules to pararealgar-like $p\text{-As}_4\text{S}_4$ [13]. The extended X-Ray absorption fine structure (EXAFS) study of photoinduced structural changes in amorphous $\text{As}_x\text{S}_{100-x}$ thin films showed that effect of the near-bandgap light illumination to the evaporated $a\text{-As}_{42}\text{S}_{58}$ and $a\text{-As}_{45}\text{S}_{55}$ films results in more disordered state and photostructural transformations are related to changes in the amorphous As-S network [14].

Raman spectroscopy of As-rich $\text{As}_{50}\text{S}_{50}$ thin films revealed pararealgar structure of $\chi\text{-As}_4\text{S}_4$, $\beta\text{-As}_4\text{S}_4$ molecules, clusters of amorphous arsenic, $\text{S}_2\text{As-AsS}_2$ and As_4S_5 structural units (s.u.), some part of $\alpha\text{-As}_4\text{S}_4$, As_4S_3 molecules, and AsS_3 pyramids [15].

The aim of the present work is a complex structural investigation of thin film surface nanolayers prepared from $\text{As}_{40}\text{S}_{60}$, $\text{As}_{45}\text{S}_{55}$, and $\text{As}_{50}\text{S}_{50}$ chalcogenide glasses using X-ray photoelectron (XPS) and Raman spectroscopy, near-bandgap laser light's influence on structural and compositional changes, and their electronic structure. In addition, the changes of surface morphology induced by laser light illumination were investigated using surface profilometry method.

Methods

High-quality optical glasses were used as the source materials for sample deposition in order to avoid the contamination in the volume of the films. The bulk $\text{As}_x\text{S}_{100-x}$ ($x = 40, 45, 50$) samples were prepared by conventional melt-quenching route in evacuated quartz ampoules from a mixture of high purity 99.999% As and S precursors. Nanolayers were prepared by thermal vacuum evaporation of appropriate bulk glass powders onto silicon and glass substrates. The thicknesses of obtained films were $\sim 0.7 \mu\text{m}$. Green diode laser operating at $\lambda = 532 \text{ nm}$ wavelength (photon energy of $\sim 2.4 \text{ eV}$) with power $p = 25 \text{ mW}$

was used to investigate the influence of the near-bandgap light irradiation on the samples of $\text{As}_{40}\text{S}_{60}$, $\text{As}_{45}\text{S}_{55}$, and $\text{As}_{50}\text{S}_{50}$ ($E_g \sim 2.4 \text{ eV}$) nanolayers. Optical irradiation was carried out with 280 mW/cm^2 intensity at ambient conditions. Laser intensity was chosen based on our previous studies of As-S glasses by means of Raman spectroscopy, mentioned above. To determine exposition of the laser illumination following experiments was done. The absorption edge of the $\text{As}_x\text{S}_{100-x}$ ($x = 40, 45, 50$) thin films and its shift under in situ illumination by green laser light was investigated using millisecond CCD spectrometer ThorLabs CCS200. Sample illumination with in situ optical spectra recording were done until saturation of the shift of the absorption edge.

Photoemission experiments were conducted by using Al $k\text{-}\alpha$ anode ($E = 1486 \text{ eV}$) as a source of X-ray. Spectra were recorded using hemispherical energy analyzer series Phoibos 100. An As 3d and S 2p core levels and valence bands (VB) were measured at normal emission geometry. Apart from this, the C 1s and O 1s core level spectra were recorded in order to normalize the positions of all spectra to a position of the graphitic peak (at 284.5 eV , [16]). C 1s core level spectra were fitted by C-C and C-O components only, and this agrees with the O-C components founded in O 1s core level spectra. Due to that C 1s and O 1s core levels would not be included in the further consideration. The CASA XPS program was used to fit core level spectra. For core level fitting, the Voigt profile components were used and Shirley background was subtracted.

Raman spectra were measured with using Renishaw system 1000 Raman spectrometer, equipped with a CCD detector. The diode laser operating at 785 nm was used as the excitation source. The measurements were made in micro-Raman configuration with using back-scattering geometry. In order to avoid stimulated by this laser photoinduced changes in the structure of the samples, the output power of the excitation source was limited by optical filters [17].

Results

Absorption Edges of $\text{As}_x\text{S}_{100-x}$ Films Under External Influence

Optical spectra of absorption edges of the $\text{As}_{40}\text{S}_{60}$, $\text{As}_{45}\text{S}_{55}$, and $\text{As}_{50}\text{S}_{50}$ films are shown in Fig. 1. As can be seen, the absorption edge of $\text{As}_{40}\text{S}_{60}$ sample shifts towards longer wavelengths when film exposed to green laser light illumination ($\lambda = 532 \text{ nm}$) with photon energy of $\sim 2.4 \text{ eV}$, which is very close to E_g of $\text{As}_{40}\text{S}_{60}$ material (Fig. 1, left). Typical red shift of the absorption edge of As-S films during the near bandgap illumination was observed earlier [5, 18]. After 45 min of laser illumination of $\text{As}_{40}\text{S}_{60}$ film, the shift becomes less and at exposure time of $\sim 150 \text{ min}$, the changes almost disappeared.

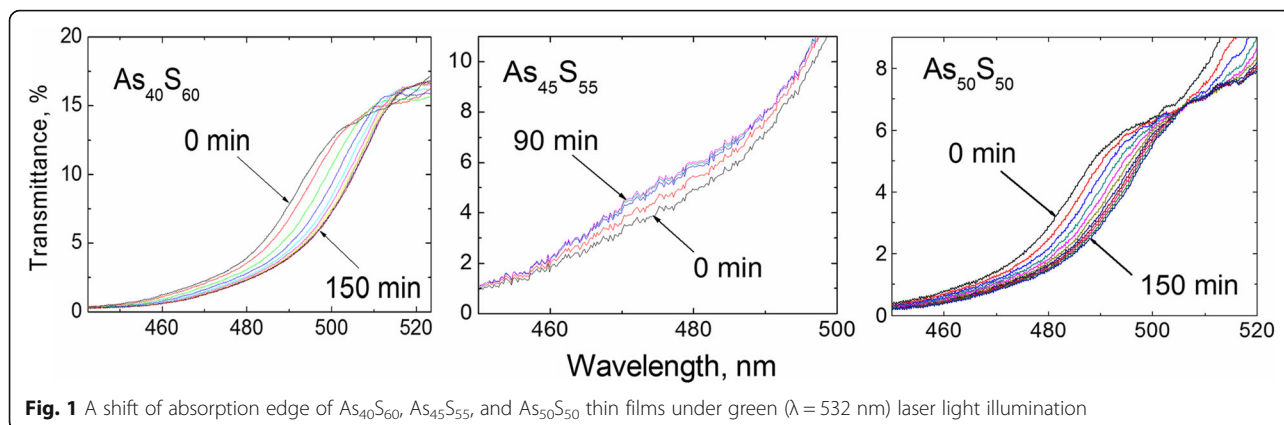


Fig. 1 A shift of absorption edge of $As_{40}S_{60}$, $As_{45}S_{55}$, and $As_{50}S_{50}$ thin films under green ($\lambda = 532$ nm) laser light illumination

A similar phenomenon was observed for the absorption edge of illuminated $As_{50}S_{50}$ film (Fig. 1, right). However, the results of the same investigation of $As_{45}S_{55}$ film demonstrate the opposite effect. For this composition, the blue shift of the absorption edge is observed under the green laser illumination and 90 min was enough to reach the saturation. The structural interpretation of this phenomenon will be provided in the next paragraph using the XPS analysis and Raman spectroscopy data.

The determined particular exposure times sufficient to saturate the changes of the absorption edges of $As_{40}S_{60}$ ($t_{exp.} = 150$ min), $As_{45}S_{55}$ ($t_{exp.} = 90$ min), and $As_{50}S_{50}$ ($t_{exp.} = 150$ min) films were used for further experiments.

XPS Spectroscopy and Valence Band Spectra of As_xS_{100-x} ($x = 40, 45, 50$) Film Surfaces

X-ray photoelectron spectroscopy can be a useful technique to investigate the surface (i.e. few topmost layers) of the materials at short-range order scale and to determine the structural units which form the investigated material. This method was successfully used to characterize the top surface nanolayer structure of the amorphous materials [19–21]. The results of XPS investigation of As_xS_{100-x} ($x = 40, 45, 50$) thin film surface nanolayers are summarized in Fig. 2. As can be seen, all S 2p core level spectra can be fitted by two components. The energy position of component 1 (and their spin-orbit split 1') allows assigning them to S– As_2 s.u. [22, 23]. It is expected that this component is a characteristic s.u. in crystalline As_2S_3 and is a main component for both stoichiometric, $As_{40}S_{60}$, and As-rich As–S glasses and films. The component 2 (and 2') can be assigned to S-rich S–SAs s.u., and it is in a good agreement with our earlier investigations and theoretical estimations [19]. The As 3d core level spectra of $As_{40}S_{60}$ nanolayers (both as-deposited and illuminated by green laser light) are fitted using three components: arsenic bonded to three sulfur atoms As– S_3 (1, 1'), arsenic bonded to two sulfur, and one arsenic atoms As– S_2 As (2, 2') and finally, arsenic

bonded to one sulfur and two arsenic atoms As– As_2S_2 (3, 3'). These assignments are based on our previous study [19] and are in excellent agreement with the published data [16, 24]. It should be noted that for the best fit of the As 3d core level spectra of $As_{45}S_{55}$ nanolayers, the fourth component is needed. The position of this component allows to interpret it as arsenic bonded to three arsenic atoms [16]. All peak component parameters are listed in Table 1.

The valence band spectra of as-deposited and illuminated by laser As_xS_{100-x} ($x = 40, 45, 50$) thin film surface nanolayers were also measured and shown in Fig. 2. The general view of these spectra for all As–S compositions is similar and correlates well with the valence band spectra of $As_{40}S_{60}$ films [25, 26]. For a better understanding of the structural changes caused by laser light illumination, differential VB spectra were constructed (Fig. 3, bottom part).

Raman Spectroscopy of $As_{40}S_{60}$, $As_{45}S_{55}$, and $As_{50}S_{50}$ Glasses and Films

Results of XPS measurements give a possibility to analyze the structure of investigated materials at micro-level (short-range order) and to determine structural units which form the substance. For a better understanding of the nature of processes and stimulated structural changes, it is necessary to investigate the structure of the samples at the extended scale range (i.e., medium range order) in order to determine the macrostructure of materials. The cage-like molecules, rings, chain-like and bigger clusters in the structure of the As–S glasses and films can clearly be detected and identified from the Raman spectra [27]. Also, the photon energy-dependent micro-Raman spectroscopy can successfully be used for monitoring the photoinduced molecular transformations [7, 12]. Therefore, this technique was used for complex investigation of the structure and induced transformations in $As_{40}S_{60}$, $As_{45}S_{55}$, and $As_{50}S_{50}$ films.

The Raman spectra of source $As_{40}S_{60}$, $As_{45}S_{55}$, and $As_{50}S_{50}$ glasses and corresponding As–S thin films are

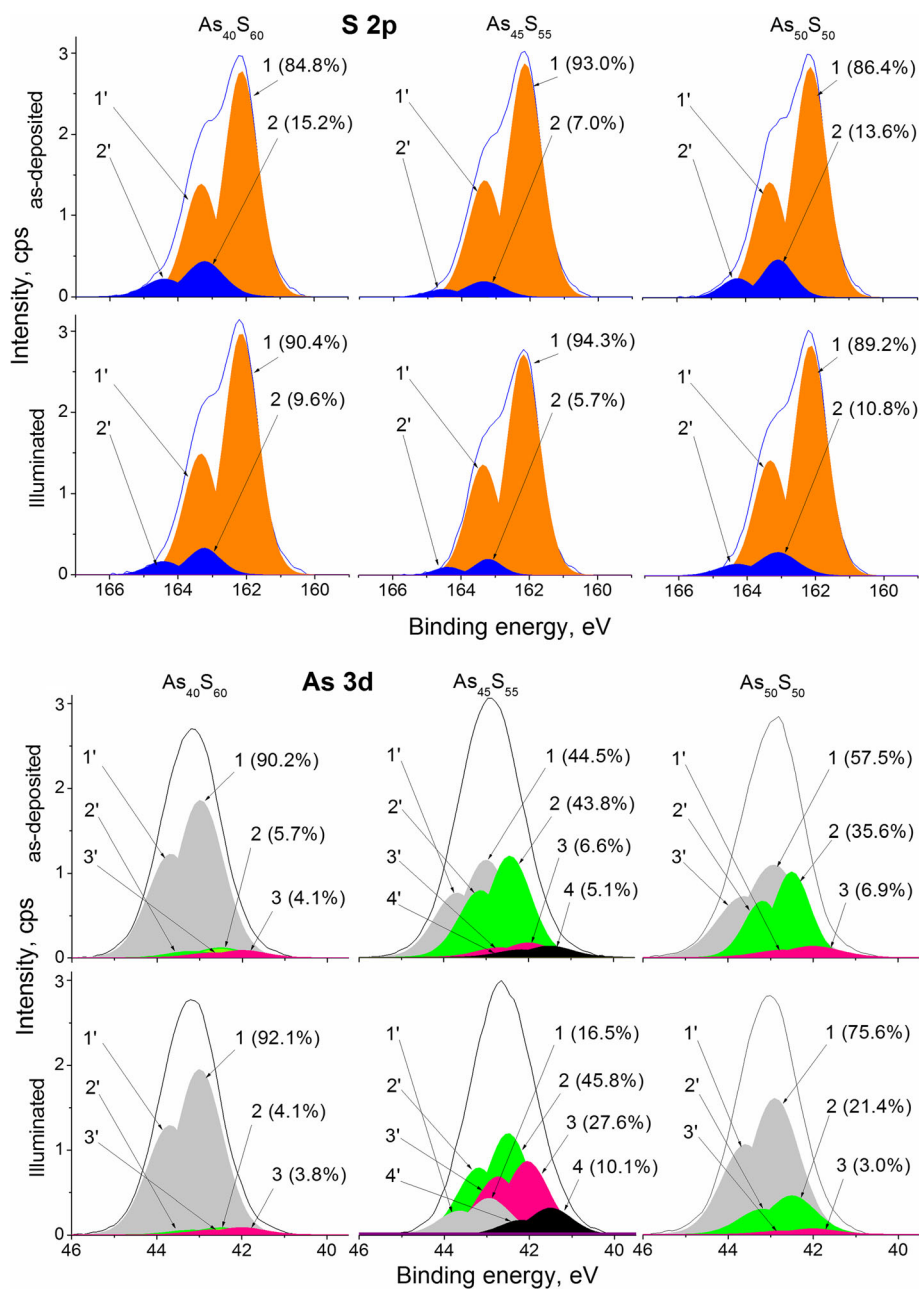


Fig. 2 S 2p and As 3d fitted core level spectra of as-deposited (top) and illuminated by green ($\lambda = 532$ nm) laser (bottom) As₄₀S₆₀, As₄₅S₅₅, and As₅₀S₅₀ thin films top nanolayers. For S 2p: 1, 2 denote 2p_{3/2} and 1', 2' denote 2p_{1/2} peaks of S–As₂ (1, 1') and S–SAs (2, 2') components; for As 3d: 1, 2, 3, 4 denote 3d_{5/2} and 1', 2', 3', 4' denote 3d_{3/2} peaks of As–S₃ (1, 1'), As–S₂As (2, 2'), As–SAs₂ (3, 3'), and As–As₃ (4, 4') components

shown in Fig. 4. As can be seen, the Raman spectra of g-As₄₀S₆₀ demonstrate a broad band with the maximum at 340 cm⁻¹ and shoulders at 310 and 380 cm⁻¹. The main band centered at 340 cm⁻¹ is a characteristic band of symmetric As–S vibrations in As₃S₃ pyramids. The shoulders at 310 and ~380 cm⁻¹ are connected with the asymmetric As–S vibrations in As₃S₃ pyramids and As–S–As vibrations of “water-like” molecule, respectively. The Raman band at 130 cm⁻¹ can be connected with

deformational vibrations of –As–S–As– and –S–As–S– structures. In addition to these bands, the very weak features at 143, 165, 186, 220, 230, and 360 cm⁻¹, connected with homopolar As–As bonds and realgar As₄S₄ inclusions, and small intensive band at 490 cm⁻¹ associated with S–S bonds are detectable in the Raman spectra of As₄₀S₆₀ glass. In contrast with the Raman spectra of stoichiometric glass, the broad band in the region of As–S valence vibrations (~300–400 cm⁻¹) in the Raman spectra

Table 1 Binding energies (BE, ± 0.1 eV) and full width at half maximum (FWHM) (± 0.05 eV) data of individual components determined from curve fitting of S 2p and As 3d XPS spectra of as-deposited and illuminated by green ($\lambda = 532$ nm) laser $As_{40}S_{60}$, $As_{45}S_{55}$, and $As_{50}S_{50}$ nanolayers

Core level/ component	$As_{40}S_{60}$				$As_{45}S_{55}$				$As_{50}S_{50}$			
	As received		Illuminated		As received		Illuminated		As received		Illuminated	
	BE	FWHM	BE	FWHM	BE	FWHM	BE	FWHM	BE	FWHM	BE	FWHM
S 2p:												
S-As ₂	162.1	1.2	162.1	1.2	162.1	1.2	162.2	1.1	162.1	1.1	162.1	1.1
S-SAs	163.2	1.3	163.2	1.1	163.3	1.3	163.2	0.9	163.1	1.1	163.1	1.3
As 3d:												
As-S ₃	43.0	1.3	43.0	1.3	43.0	1.3	42.9	1.2	42.9	1.5	42.9	1.3
As-S ₂ As	42.5	1.3	42.5	1.3	42.4	1.2	42.5	1.2	42.5	1.0	42.5	1.3
As-SAs ₂	42.0	1.3	42.0	1.3	42.0	1.3	42.1	1.2	42.0	1.5	42.0	1.3
As-As ₃	-	-	-	-	41.5	1.3	41.5	1.2	-	-	-	-

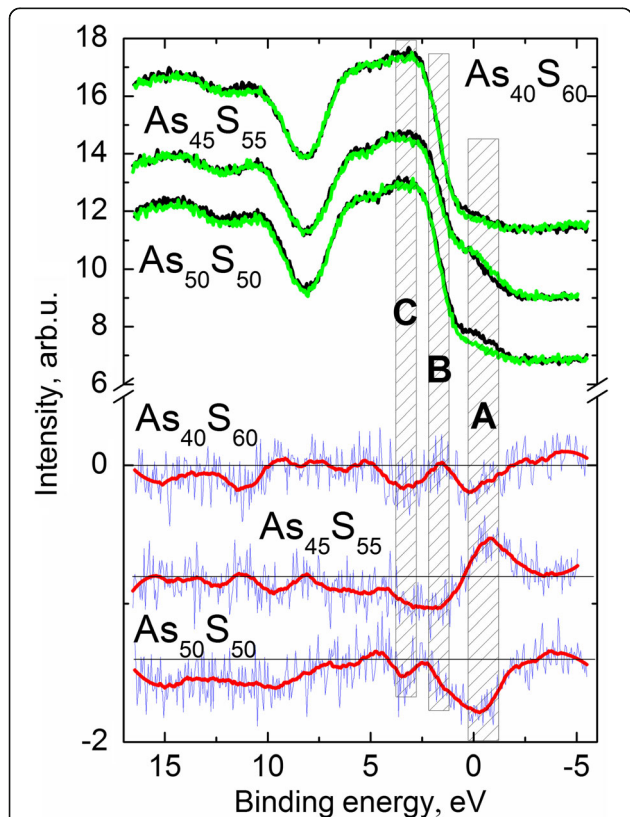


Fig. 3 Valence band spectra of as-deposited (black lines) and illuminated by green ($\lambda = 532$ nm) laser light (green lines) $As_{40}S_{60}$, $As_{45}S_{55}$, and $As_{50}S_{50}$ thin film nanolayers (top part). Differential (illuminated minus as received) original (blue spiked lines) and smoothed (red thick lines) spectra (bottom part)

of corresponding $As_{40}S_{60}$ films clearly show the double-peak structure. The simultaneous increases in intensities of 360 cm^{-1} Raman band and bands in the region of molecular and As-As valence band vibrations ($100\text{--}300\text{ cm}^{-1}$) can indicate the increasing of the concentration of cage-like As_4S_4 molecules in $As_{40}S_{60}$ films in comparison with those found in the structure of corresponding target glass. As can be seen from intensities of 490 cm^{-1} bands (Fig. 4, curve 1), the concentration of homopolar S-S bonds in the structure of $As_{40}S_{60}$ films is larger than in $As_{40}S_{60}$ glass. At the same time, the new band at $\sim 270\text{ cm}^{-1}$ is detected in the Raman spectra of $As_{40}S_{60}$ films. This band is assigned to the vibrations in As-rich As_4S_3 cage-like molecules [28].

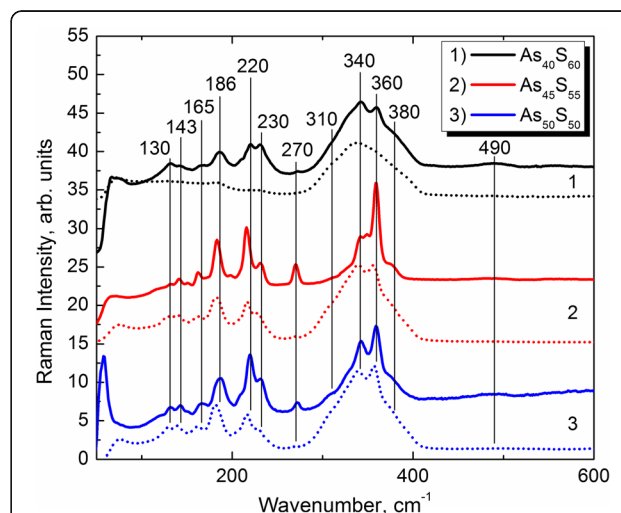


Fig. 4 Raman spectra of $As_{40}S_{60}$ (1), $As_{45}S_{55}$ (2), and $As_{50}S_{50}$ (3) target glasses (dotted line) and corresponding thin films (solid line)

The Raman spectra of $As_{45}S_{55}$ and $As_{50}S_{50}$ glasses are very similar (Fig. 4, curves 2 and 3). The main contributions in the Raman spectra of both glasses originate from As_4S_4 cage-like molecules. Weak band at 270 cm^{-1} characteristic of As_4S_3 molecules was detected, and no S–S bonds (490 cm^{-1} Raman mode) were found for both glass compositions. The difference in the Raman spectra of $As_{45}S_{55}$ and $As_{50}S_{50}$ glasses is connected with redistribution of 340 and 360 cm^{-1} band intensities only. In contrast with the glasses, the Raman spectra of $As_{45}S_{55}$ and $As_{50}S_{50}$ thin films are different. The main differences are connected with the intensity of Raman band at 270 and 360 cm^{-1} . These bands are more intensive in the Raman spectra of $As_{45}S_{55}$ films indicating the drastic separations of cage-like As_4S_3 and As_4S_4 molecules from pyramidal network. Also, the very weak band at $\sim 490\text{ cm}^{-1}$ (S–S bonds) is detected in the Raman spectra of both $As_{45}S_{55}$ and $As_{50}S_{50}$ films.

Discussion

Atomic Stoichiometry of As–S films

From the core level spectra of As_xS_{100-x} ($x = 40, 45, 50$) thin film surface nanolayers which are shown in Fig. 3, the atomic concentrations and As to S ratios of as-deposited and illuminated by green laser light samples were calculated. The appropriate values are given in Table 2.

As it can be seen, the thermal evaporation of the bulk chalcogenide glass of $As_{40}S_{60}$ composition causes the $As_{42.9}S_{57.1}$ composition of deposited thin film. Laser light illumination with near-bandgap photon energy leads to further slight arsenic enrichment. More As-rich thin film in comparisons with target composition is obtained when the $As_{45}S_{55}$ glass is evaporated (see Table 2). Further

arsenic content increment from 48.9% in the as-deposited sample to 51.0% in the sample illuminated by a green laser light during 90 min takes place. Correspondingly, the appropriate As to S ratio is changed from 0.96 to 1.04. Unexpectedly, the thermal evaporation of $As_{50}S_{50}$ glass leads to deposition of thin film with the As/S ratio which is less than for the bulk glass ($As_{45.4}S_{54.6}$ composition) (Table 2). The laser treatment of this sample causes small arsenic enrichment, but the ratio between As and S remains far from the appropriate value in the bulk glass.

Such deviations of the thin film stoichiometry from the bulk glasses and further changes to them under the external (laser) influence with photon energy close to the band gap of investigated materials can be understood and explained from a detailed component analysis [29, 30].

Component Analysis of As_xS_{100-x} ($x = 40, 45, 50$) Thin Films Under External Influence

As mentioned above, the fit of core level spectra of all films (before and after treatment) demonstrates the presence of structural units with homopolar bonds (see Fig. 2). Because of sulfur is twofold coordinated and arsenic is threefold coordinated in As–S system, the $As_{40}S_{60}$ films in ideal composition should demonstrate the water-like S– As_2 and pyramidal As– S_3 components only in their S 2p and As 3d core level spectra, respectively. However, the homopolar As–As bonds were detected in the As 3d core level spectra of all As_xS_{100-x} ($x = 40, 45, 50$) nanolayers which is expected from As-enrichment ($x > 40$ at. % As) of their top surface. In accordance with this for the $As_{40}S_{60}$ composition, it was found of 5.7% s.u. which are assigned to arsenic bonded to two sulfur and one arsenic atoms, and of 4.1% s.u. which mean the presence of the arsenic

Table 2 Atomic concentrations, As/S ratio of $As_{40}S_{60}$, $As_{45}S_{55}$, and $As_{50}S_{50}$ nanolayers calculated from XPS data (the values of As/S ratio for the bulk glasses are given in parentheses for comparison) and contribution (area, $\pm 5\%$) to the core level of each doublet of individual components determined from curve fitting of S 2p and As 3d XPS spectra

Element/ Core level/ Component	$As_{40}S_{60}$		$As_{45}S_{55}$		$As_{50}S_{50}$	
	As-deposited	Illuminated	As-deposited	Illuminated	As-deposited	Illuminated
As, %	42.9	43.0	48.9	51.0	45.4	45.8
S, %	57.1	57.0	51.1	48.9	54.6	54.2
As/S	0.75 (0.67)	0.75	0.96 (0.82)	1.04	0.83 (1)	0.84
S 2p:						
S– As_2 , %	84.8	90.4	93.0	94.3	86.4	89.2
S–SAs, %	15.2	9.6	7.0	5.7	13.6	9.8
As 3d:						
As– S_3 , %	90.2	92.1	44.5	16.5	57.5	75.6
As– S_2 As, %	5.7	4.1	43.8	45.8	35.6	21.4
As– SA_2 , %	4.1	3.8	6.6	27.6	6.9	3.0
As– As_3 , %	–	–	5.1	10.1	–	–

bonded to one sulfur and two arsenic atoms (peaks 2, 2' and 3, 3', respectively). The contributions of these two As-rich components are much significant in As 3d core level spectra of $\text{As}_{45}\text{S}_{55}$ film surface (see Table 2). Moreover, the fourth component, As–As₃ is appeared with 5.1% contribution, which is reasonable for calculated composition ($\text{As}_{51.1}\text{S}_{48.9}$). Finally, the thin film obtained by thermal evaporation of the $\text{As}_{50}\text{S}_{50}$ target glass contains 35.6% of As–S₂As s.u. and 6.9% of As–SAs₂ s.u. apart from the pyramidal one.

Despite to arsenic enrichment of all three as-deposited As–S samples in comparison with the stoichiometric composition, the S 2p core level spectra contain a component with the homopolar S–S bond (Fig. 2). There is a strong correlation between the As to S ratio of as-deposited samples and the percentage of S–SAs s.u. in the appropriate S 2p core levels. However, the further explanation of the existence of S–S bonds in As-rich structures is needed.

The properties and micro structure of vapor-deposited films depend on the deposition methods and conditions. Therefore, the resulting film structure can be different from the structure of the corresponding bulk glasses as established earlier [31]. The As–As bond formation in the as-deposited As_2S_3 film was detected with using X-ray diffraction technique. On the basis of the arsenic enrichment of the film and detected by mass spectroscopy fragmentation into S₂ and As₄S₄ during the evaporation of the bulk As_2S_3 glass, the formation of a sheet-like open structure of the film is supposed [31]. Also, it is pointed out that the As–As bonds may be incorporated as S₂As–AsS₂ units, as in As₄S₄ molecules as determined using extended X-ray absorption edge fine structure and Raman and IR spectroscopy. Apart from this, the dominance of As₄S₄ and sulfur molecules in as-deposited films were shown by neutron diffraction study [31]. The mass spectrometry study shows the presence of S₂ and different AsS particles in the gas phase of As–S system [32]. Therefore, the presence of S–S s.u. (S 2p spectra) in the structure of all As–S films and the appearance of As–S₂As s.u. in the As 3d core level spectra of even stoichiometric $\text{As}_{40}\text{S}_{60}$ composition can be understood. Moreover, apart from the composition of the target glass, the type of molecules in vapor plays a significant role in the formation of the film composition and structure. This way, the differences in compositions of the films and corresponding source materials can be explained. Additional support of mentioned As-enrichments of top surface As–S nanolayers can be confirmed by Raman spectroscopy. In particular, the biggest arsenic enrichment is found for As–S film deposited from $\text{As}_{45}\text{S}_{55}$ glass where the most significant contribution of As-rich As₄S₃ molecules is detected (Fig. 4, curve 2).

Near-bandgap laser light illumination of $\text{As}_x\text{S}_{100-x}$ ($x = 40, 45, 50$) samples causes decreasing of the contribution of components with the homopolar S–S bonds in all the samples (Table 2). This phenomenon was observed in our previous investigations [19] and was explained by the processes of the structural ordering under the laser light illumination. In addition, the decreasing of components with homopolar As–As bonds in the structure of $\text{As}_{40}\text{S}_{60}$ and $\text{As}_{50}\text{S}_{50}$ nanolayers under the near-bandgap laser light illumination was observed (Fig. 2, Table 2). This is in accordance with the results of our in situ under-bandgap laser light illumination of As_2S_3 nanolayers [19]. The decreasing of concentration of homopolar As–As bonds in the structure of $\text{As}_{40}\text{S}_{60}$ and $\text{As}_{50}\text{S}_{50}$ films under laser illumination correlates well with the partial disappearance of the S–S bonds and creation of new As–S bonds.

However, the different behavior in compositional and structural changes under laser illumination was observed for $\text{As}_{45}\text{S}_{55}$ films. In contrast with $\text{As}_{40}\text{S}_{60}$ and $\text{As}_{50}\text{S}_{50}$ nanolayers, the increasing of concentration of components with As–As bonds was detected in $\text{As}_{45}\text{S}_{55}$ films as a result of the near-bandgap laser light illumination (Fig. 2, Table 2). Similar increasing was also detected in As_2S_3 nanolayers when over-bandgap laser light illumination was applied [19]. This effect was explained by atomic movement of As from deeper to top layers under the laser treatment, leading to As-enrichment of the sample surface. Such movement appears due to a creation of electric field gradient which is driving force on dipoles and charged defects resulting in mass transport.

The larger magnitude of laser-induced changes in As–S system was found for As-rich compositions with As₄S₄ inclusions [7]. It should be noted here that XPS spectroscopy reveals the most As-enriched composition of As–S film prepared from $\text{As}_{45}\text{S}_{55}$ glass among studied $\text{As}_x\text{S}_{100-x}$ ($x = 40, 45, 50$) films. Moreover, the significant As enrichment of the $\text{As}_{45}\text{S}_{55}$ sample was confirmed by Raman spectroscopy (Fig. 4, curve 2) where the 270 cm⁻¹ Raman band characteristic of As₄S₃ molecules show maximal intensity. In this manner, the specific behavior and the structural rearrangement of the $\text{As}_{45}\text{S}_{55}$ nanolayers are conditioned by a considerable number of As-rich s.u., particularly As₄S₃. This can stimulate laser-induced mass transport effect resulting in further arsenic enrichment of the sample surface.

Valence Band Spectra of As–S films

In general, the valence band can be determined as the highest range of electron energies which can be occupied at absolute zero temperature [33]. According to Mott and Devis model, the valence band of amorphous materials contains the states formed by defect centers [34]. For the As–S system, the top of the VB is formed

by lone-pair 3p electrons of sulfur (at ~ 3 eV), as 4p and S 3p levels (bonding electrons) are situated at ~ 5 and ~ 7 eV, respectively. Next energy band is located lower than 10 eV and formed by the S 3s and As 4s electrons. These data were confirmed by DFT electronic structure calculations of As- and S-centered s.u. [19].

A qualitative comparison of the VB spectra of As_2S_3 nanolayers investigated in situ [19] with the VB spectra of $\text{As}_x\text{S}_{100-x}$ ($x = 40, 45, 50$) films show the differences connected with the presence of additional states at energies ranged from -1.7 to 0.6 eV (Fig. 3). According to the calculated data, the formation of homopolar As–As bonds leads to the appearance of the energy levels in the band gap of the As–S structures [35, 36]. The concentration of As–As bonds in $\text{As}_x\text{S}_{100-x}$ ($x = 40, 45, 50$) films was found to increase in order: $\text{As}_{40}\text{S}_{60}$, $\text{As}_{50}\text{S}_{50}$, and $\text{As}_{45}\text{S}_{55}$ (Table 2). Taking into account, the changes of the concentrations of s.u. with homopolar As–As bonds induced by laser treatment (decreasing for $\text{As}_{40}\text{S}_{60}$, $\text{As}_{50}\text{S}_{50}$ composition and increasing for $\text{As}_{45}\text{S}_{55}$ structure) (Table 2) and intensities of electronic states in the VB spectra of As–S films (from -1.7 to 0.6 eV) (Fig. 3) can be assumed that they are formed by structural units with As–As bonds.

The main changes in the electronic structure of As–S samples induced by laser light illumination can be selected (highlighted regions in Fig. 3). The changes in these regions (denoted as A, B, and C) can clearly be seen from the differential valence band spectra (Fig. 3, bottom). The right highlighted region (A) in the differential VB spectra of $\text{As}_x\text{S}_{100-x}$ ($x = 40, 45, 50$) films points out to the changes of the states in the band gap of the structures. Middle highlighted region (B) indicates that the band gap decreases in the As–S samples of the $\text{As}_{40}\text{S}_{60}$ and $\text{As}_{50}\text{S}_{50}$ compositions and increases in the $\text{As}_{45}\text{S}_{55}$ structure under the near-bandgap laser light illumination. It should be noted that these results correlate with the shift of absorption edge measurements. And finally, left marked region (C) demonstrates common decreasing of the concentration of S–S homopolar bonds in all As–S films under laser treatment (see Figs. 2 and 3, Table 2).

Profilometry Analysis of Laser Induced Relief Formation in $\text{As}_x\text{S}_{100-x}$ ($x = 40, 45, 50$) Films

As it was mentioned above, the increasing of the components with the As–As bonds under the near-bandgap laser light illumination takes place due to a creation of electric field gradient resulting in mass transport. In order to examine of this effect, the additional experiments were performed. The as-deposited films of all three compositions were illuminated by green laser light through the copper mesh with grating period of $60 \mu\text{m}$ during time sufficient for saturation of shift of absorption edge,

measured previously (see previous chapter). Then, the surface of irradiated As–S samples was examined by AMBIOS XP-1 type profilometer with 10 nm vertical resolution (stylus tip radius— $2.5 \mu\text{m}$). For the profilometer measurements, a 0.5 mg load was applied. This load was small enough to make the accurate profiling without destroying the surface morphology. Results are shown in Fig. 5.

As can be seen, the laser light illumination does not change the shapes of the surfaces of both $\text{As}_{40}\text{S}_{60}$ and $\text{As}_{50}\text{S}_{50}$ thin films. Thus, it can be concluded that laser illumination was not influenced on morphology of the surface of these samples. However, the different behavior in laser-induced transformations and surface morphology changes was discovered for $\text{As}_{45}\text{S}_{55}$ thin film (see Fig. 5, curve 2). It is clearly seen that under the laser light illumination the “wave-like” relief on the surface of $\text{As}_{45}\text{S}_{55}$ film is formed. The parameters of the induced grating can be seen in the insert of Fig. 5. This relief corresponds to the period of the mesh grating.

Taking into account that the $\text{As}_{45}\text{S}_{55}$ composition demonstrates peculiarities and opposite induced phenomena (shift of the absorption edge, stoichiometry and local structure changes, untypical VB shift, and shape changes) in comparison with the $\text{As}_{40}\text{S}_{60}$ and $\text{As}_{50}\text{S}_{50}$ thin films and contains the largest concentration of As_4S_3 cage-like molecules, it can be concluded that the presence of polar As_4S_3 molecules (which are sensitive to the electric field generated by the laser) is responsible for observed laser-induced mass transport effect. The drift and re-arrangements of this molecules results in photoexpansion of illuminated areas. The observed phenomena can be used for optical grating formation, controlled laser surface modification, laser induced surface activation, etc.

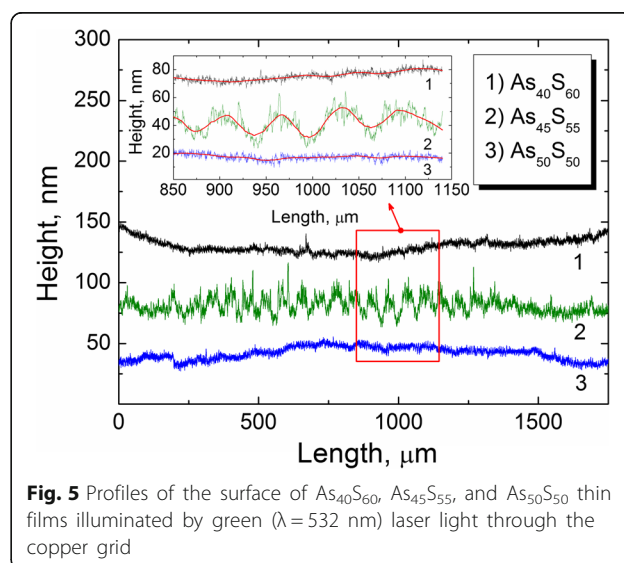


Fig. 5 Profiles of the surface of $\text{As}_{40}\text{S}_{60}$, $\text{As}_{45}\text{S}_{55}$, and $\text{As}_{50}\text{S}_{50}$ thin films illuminated by green ($\lambda = 532$ nm) laser light through the copper grid

Conclusions

The local and molecular structures of As_xS_{100-x} ($x = 40, 45, 50$) thin film surface and their transformations induced by coherent near-bandgap laser illumination have been investigated using XPS and Raman spectroscopy. The optical properties and induced transformation of surface morphology of As–S nanolayers have been also studied by means of absorption edge spectroscopy and 2D profilometry.

A significant difference in surface stoichiometry between amorphous As–S films and composition of corresponding target glasses was established, and it was found to be related with the peculiarities in molecular constituent of gas phase during the deposition process, indicating that the type of molecules in vapor plays a crucial role in resulting film composition. Near-bandgap laser illumination decreases the concentration of the homopolar S–S bonds in the structure of all As_xS_{100-x} ($x = 40, 45, 50$) nanolayers. However, the decreasing of the concentration of homopolar As–As bonds upon laser illumination was observed in the structure of $As_{40}S_{60}$ and $As_{50}S_{50}$ films only. In contrast with $As_{40}S_{60}$ and $As_{50}S_{50}$ films, the contribution of As– S_2 As and As– SAs_2 components and appearance of a new As-rich As– As_3 s.u. in the structure of $As_{45}S_{55}$ thin film during laser illumination were detected. Moreover, this particular film ($As_{45}S_{55}$) demonstrates peculiarities in laser-induced shift of the absorption edge, in Raman spectra, and finally, in effect of induced surface morphology transformation.

The results of Raman investigation of As–S films indicate the presence of As-rich As_4S_3 molecules in the structure of $As_{45}S_{55}$ nanolayers in largest concentration among studied samples. Therefore, the As_4S_3 molecules were found to be responsible for drastic difference in behavior of absorption edge spectra and surface morphology transformation of $As_{45}S_{55}$ nanolayers during near-bandgap laser illumination. The presence of these As_4S_3 structures in the structure of $As_{45}S_{55}$ nanolayers results in laser-induced mass transport effect observed for this material and can be useful for optical grating formation and related external nanofabrication technologies.

Abbreviations

BE: Binding energy; ChG: Chalcogenide glass; FWHM: Full width at half maximum; VB: Valence bands; XPS: X-ray photoelectron spectroscopy

Acknowledgements

O.K. and R.H. gratefully acknowledge support from the Hungarian Academy of Sciences within the Domus Hungarica Scientiarum et Artium. The work/publication is supported by the GINOP-2.3.2-15-2016-00041 project. The project is co-financed by the European Union and the European Regional Development Fund.

Authors' Contributions

All authors (OK, RH, ACh, VT, MV, and VM) equally contributed in developing the general idea and methodological aspects of performed investigation. OK, RH, and VM prepared the source glasses and synthesized As_xS_{100-x} thin films of different ($x = 40, 45, 50$) compositions. OK, VT, and ACh performed the XPS, absorption edge spectroscopy, and profilometer measurements to characterize

the samples. RH and MV performed the Raman spectroscopy measurements and spectral interpretation. VM carried out the general control of the processing and analysis of the results. All authors read and approved the final manuscript.

Competing Interests

The authors declare that they have no competing interests.

Author details

¹Uzhhorod National University, Pidhirna Str. 46, Uzhhorod 88000, Ukraine.

²Institute for Nuclear Research, Hungarian Academy of Sciences, Debrecen H-4001, Hungary. ³Wigner Research Centre for Physics, Hungarian Academy of Sciences, Budapest 1121, Hungary.

Received: 29 December 2016 Accepted: 13 February 2017

Published online: 27 February 2017

References

- Mott NF, Davis EA (1971) Electronic processes in non-crystalline materials. Oxford Univ. Press, London
- Felts A (1986) Amorphous and vitreous inorganic solids. Mir, Moscow, in Russian
- Tanaka K, Ohtsuka Y (1979) Composition dependence of photo-induced refractive index changes in amorphous AsS films. *Thin Solid Films* 57:59–64
- Elliott SR (1986) A unified model for reversible photostructural effects in chalcogenide glasses. *J Non-Cryst Solids* 81:71–98
- Hisakuni H, Tanaka K (1994) Giant photoexpansion in As_2S_3 glass. *Appl Phys Lett* 65:2925–2927
- Andriesh AM, Bykovskii YA, Kolomeiko EP, Makovkin AV, Smirnov VL, Shmal'ko AV (1977) Waveguide structures and functional elements of integrated optics systems based on volume holographic gratings in thin As_2S_3 films. *Sov J Quantum Electron* 7(3):347
- Holomb R, Mateleshko N, Mitsa V, Johansson P, Matic A, Veres M (2006) New evidence of light-induced structural changes detected in As-S glasses by photon energy dependent Raman spectroscopy. *J Non-Cryst Sol* 352:1607–1611
- Eisenberg NP, Manevich M, Klebanov M, Shutina S, Lyubin V (1995) Fabrication of microlens array for the IR by lithographic processes using an inorganic chalcogenide photoresist. *Proc SPIE-Int Soc Opt Eng* 2426:235–241
- Kim HM, Jeong JW, Kwak CH, Lee SS (1995) Binary phase spatial modulation using photoinduced anisotropy in amorphous As_2S_3 thin films. *Appl Opt* 34:6008–6011
- Klebanov M, Shutina S, Bar I, Lyubin V, Rosenwaks S, Volterra V (1995) Films of chalcogenide glasses as perspective materials for optical information recording. *Proc. SPIE-Int Soc Opt Eng* 2426:198–209
- Mitsa V, Holomb R, Veres M, Marton A, Rosola I, Fekeshgazi I, Koós M (2011) Non-linear optical properties and structure of wide band gap non-crystalline semiconductors. *Phys Status Solidi C* 9:2696–2670
- Holomb R, Mitsa V, Petrachenkov O, Veres M, Stronski A, Vlček M (2011) Comparison of structural transformations in bulk and as-evaporated optical media under action of polychromatic or photon-energy dependent monochromatic illumination. *Phys Status Solidi C* 8:2705–2708
- Holomb R, Mitsa V, Johansson P, Mateleshko N, Matic A, Veresh M (2005) Energy-dependence of light-induced changes in g- $As_{45}S_{55}$ during recording the micro-Raman spectra. *Chalcogenide Letts* 2:63–69
- Weiqing Z, Lee JM, Sayers DE, Paesler MA (1989) An exafs study of compositional trends and photo-induced structural changes in amorphous As_2S_3 thin films. *J Non-Cryst Sol* 114:43–45
- Nmec P, Jedelský J, Frumar M, Vlček M (2005) Structure of pulsed-laser deposited $As_{50}S_{50}$ amorphous thin films. *J Optoelect Adv Mat* 7:2635
- Wanger CD, Riggs WM, Davis LE, Moulder JF, Muilenberg GE (1979) Handbook of x-ray photoelectron spectroscopy. Perkin-Elmer Corp., Physical Electronics Division, Eden Prairie, Minnesota
- Kondrat O, Popovich N, Holomb R, Mitsa V, Petrachenkov O, Koós M, Veres M (2010) Ab initio calculations and the effect of atomic substitution in the Raman spectra of As(Sb, Bi) $_2S_3$ films. *Phys Stat Sol C* 7:893–896
- Zakery A, Elliott SR (2003) Optical properties and applications of chalcogenide glasses: a review. *J Non-Cryst Solids* 330:1–12
- Kondrat O, Holomb R, Popovich N, Mitsa V, Veres M, Csik A, Feher A, Tsud N, Vondráček M, Matolín V, Prince KC (2015) In situ investigations of laser and thermally modified As_2S_3 nanolayers: synchrotron radiation photoelectron spectroscopy and density functional theory calculations. *J Appl Phys* 118:225307–7

20. Kondrat O, Holomb R, Popovich N, Mitsa V, Veres M, Csik A, Tsud N, Matolin V, Prince KC (2015) Local surface structure and structural properties of As-Se nanolayers studied by synchrotron radiation photoelectron spectroscopy and DFT calculations. *J Non-Cryst Solids* 410:180–185
21. Duk-Yong C, Madden S, Rode A, Wang R, Luther-Davies B (2007) Nanoscale phase separation in ultrafast pulsed laser deposited arsenic trisulfide (As_2S_3) films and its effect on plasma etching. *J Appl Phys* 102:083532–083535
22. Petkov K, Krastev V, Marinova TS (1994) XPS study of amorphous As_2S_3 films deposited onto chromium layers. *Surf Interface Anal* 22:202–205
23. Soma M, Tanaka A, Seyama H, Satake K (1994) Characterization of arsenic in lake sediments by X-ray photoelectron spectroscopy. *Geochim Cosmochim Acta* 58:2743–2745
24. Kovalskiy A, Cech J, Vlcck M, Waits CM, Dubey M, Heffner WR, Jain H (2009) Chalcogenide glass e-beam and photoresists for ultrathin grayscale patterning, RID A-8566-2008, RID A-2506-2009. *J Micro/Nanolith MEMS MOEMS* 8:043012–043012
25. Bullen HA, Dorko MJ, Oman JK, Garrett SJ (2003) Valence and core-level binding energy shifts in realgar (As_4S_4) and pararealgar (As_4S_4) arsenic sulfides. *Surf Sci* 531:319–328
26. Kovalskiy A, Neilson JR, Miller AC, Miller FC, Vlcck M, Jain H (2008) Comparative study of electron- and photo-induced structural transformations on the surface of $As_{35}S_{65}$ amorphous thin films. *Thin Solid Films* 516:7511–7518
27. Holomb R, Veres M, Mitsa V (2009) Ring-, branchy-, and cage-like As_nS_m nanoclusters in the structure of amorphous semiconductors: *ab initio* and Raman study. *J Optoelect Adv Mat* 11:917–923
28. Holomb RM, Mitsa VM (2004) Simulation of Raman spectra of As_xS_{100-x} glasses by the results of *ab initio* calculations of As_nS_m clusters vibrations. *J Optoelect Adv Mat* 6:1177–1184
29. Kondrat O, Popovich N, Holomb R, Mitsa V, Lyamayev V, Tsud N, Cháb V, Matolin V, Prince KC (2012) Laser induced changes of $As_{50}Se_{50}$ nanolayers studied by synchrotron radiation photoelectron spectroscopy. *J Thin Solid Films* 520:7224–7229
30. Kondrat O, Popovich N, Holomb R, Mitsa V, Lyamayev V, Tsud N, Cháb V, Matolin V, Prince KC (2012) Synchrotron radiation photoelectron spectroscopy studies of self-organization in $As_{40}Se_{60}$ nanolayers stored under ambient conditions and after laser irradiation. *J Non-Crystalline Solids* 358:2910–2916
31. Koto W, Binod K, Rai AK (1988) Effect of deposition rate on structure and properties of As_2S_3 film. *Thin Solid Films* 161:139–147
32. Popescu AA, Savastru D, Ciobanu M, Miclos S, Dolghier VT (2011) Mass-spectrometric studies of vitreous As_2S_3 . *J Optoelect Adv Mat* 13:1193–1198
33. Mott NF, Davis EA (1979) *Electronic processes in non-crystalline materials*. Clarendon, Oxford
34. Mott NF, Davis EA, Street RA (1975) States in the gap and recombination in amorphous semiconductors. *Philos Mag* 32:961–996
35. Shchurova TN, Savchenko ND, Kondrat AB, Opachko II (2006) Auger analysis and simulation of electronic states for $Ge_{33}As_{12}Se_{55}$ - *p*-Si heterojunction. *Surf Interface Anal* 38:448–451
36. Shchurova TN, Savchenko ND, Kondrat AB, Popovych KO, Rubish VM, Leising G (2008) Simulation of the surface bending of energy band for binary chalcogenide semiconductors. *Photoelectronics* 17:104–107

Submit your manuscript to a SpringerOpen® journal and benefit from:

- Convenient online submission
- Rigorous peer review
- Immediate publication on acceptance
- Open access: articles freely available online
- High visibility within the field
- Retaining the copyright to your article

Submit your next manuscript at ► springeropen.com
